Desk top \ N-C Stainless steel oxidation \ Manuscript oxidation of metals Final Revision 12 March 2010
Changes made after David's latest comments
last edited: March 24, 2010 (12:17pm)

Journal article for: OXIDATION of METALS

Oxidation characteristics of Fe-18Cr-18Mn-stainless steel alloys

James Rawers, U.S. Department of Energy,
National Energy Technology Laboratory, Albany, Oregon
Rawers@NETL.DOE.GOV

ABSTRACT

Air oxidation studies of Fe-18Cr-18Mn stainless steels were conducted at 525°C, 625°C, and 725°C. Alloys were evaluated with respect to changes in oxidation properties as a result of interstitial additions of nitrogen and carbon and of minor solute additions of silicon, molybdenum, and nickel. Interstitial concentrations possibly had a small, positive effect on oxidation resistance. Minor solute additions significantly improved oxidation resistance but could also reduce interstitial solubility resulting in formation of chromium carbides. Loss of solute chromium resulted in a slight reduction in oxidation protection. Oxidation lasting over 500 hours produced a manganese rich, duplex oxide structure: an outer sesquioxide and an inner spinel oxide.

INTRODUCTION:

Few studies of high temperature properties of manganese rich austenitic iron-chromium alloys have been published **[1, 2, 3, 4, 5]**. Oxidation studies of these alloys with elevated concentrations of interstitial nitrogen and carbon are even rarer. This study was designed to evaluate the oxidation characteristics of Fe-18Cr-18Mn alloys that had been interstitially strengthened with nitrogen and carbon and alloyed with minor solid-solution alloyed.

The economy of Fe-Cr-Mn alloys is favorable because the less-expensive, manganese replaces the more-expensive nickel as the austenite-forming element. For oxidation/corrosion protection, nickel-based and manganese-based stainless steel alloy systems have similar chromium concentrations, normally above 18 weight percent. This study is a preliminary investigation to determine how addition of nitrogen and carbon interstitials affects oxidation properties of iron-chromium-manganese alloys, and if oxidation resistance of these alloys can be further improved by minor, solid-solution, addition of silicon, molybdenum and nickel.

EXPERIMENTAL PROCEDURE:

Six 5 kilogram ingots of high-interstitial stainless steel were induction melted in a nitrogen environment (**TABLE 1**). Ingots were normalized at 1150°C for 24 hours then hot-worked at 1100°C using 20 to 30% reductions into sheets approximately 2.5 millimeters thick. Test samples were cut for microstructure characterization: X-ray diffraction and optical and scanning electron microscopy. Microstructure, mechanical, and wear properties of these alloys have been published in **references 6, 7, and 8.**

For oxidation tests, samples were sectioned from the hot-worked and annealed sheets into coupons, 25 mm x 25 x mm x 2.5mm, and metallographically polished to a 600 micron finish. Surfaces were cleaned with alcohol and oven dried at 75°C overnight. Oxidation tests were conducted on duplicate samples in an open atmosphere, box furnace with temperature controls ±2°C. To determine oxidation rate, samples were weighed periodically: 15 data points over 1244 hours at 525°C, 14 data points over 1244 hours at 625°C, 15 data points over 670 hours at 725°C. Weighing times were selected to be equally spaced on a logarithmic time scale. Coupons were removed from further testing if they showed a loss of weight in two consecutive weighings (**TABLE II**).

Post oxidation examination included X-ray diffraction of the oxide surface as well as optical and scanning electron microscopic examination. Scanning electron microscopic analysis included energy-dispersive, elemental analysis of the oxide surface.

Results:

Previous studies have characterized microstructure [8], mechanical [6], and wear properties of the alloys in this study [7]. The base composition, Fe-18Cr-18Mn, is a duplex fcc-bcc phase alloy. Alloying with nitrogen and carbon stabilizes the fcc phase. Additions of minor alloying elements, silicon, molybdenum, and nickel, did not change the solubility of nitrogen interstitials. However, minor alloy addition of silicon reduces carbon solubility [8] resulting in micron size, uniform dispersion of $Cr_{23}C_6$ precipitates. **(TABLE 1)**

All six Fe-Cr-Mn alloys survived 1200 hours at both 525°C and 625°C, and alloys with minor alloy additions survived 640 hours at 725°C. For samples without minor alloy additions, spalling began after several hundred hours at 725°C.

For each temperature, oxidation weight change data were evaluated using:

EQ.1 $\delta[(\text{grams/cm}^2)]^2 = k * t.$

Data for all three temperatures were then combined and evaluated using:

EQ.2 $\delta[(\text{grams/cm}^2)]^2 = a * \exp(-Q/RT) * t.$

$\delta(\text{grams/cm}^2)$ = sample weight gain per cm^2 at time t and temperature T

t = time hours, R = gas constant, T = temperature Kelvin,

a & k = material oxidation rate constants to be determined,

Q/R = oxide free energy to be determined.

Nonlinear statistical regression analysis was used to fit the oxidation-weight gain data. Initially, time in EQ.1 and EQ.2 was fitted with an exponent that was allowed to vary. However, the time exponent was consistently 1.0 ±0.02 with a statistical certainty of R^2 value greater than 0.99. The data reported in **TABLE II** is for a constant time exponent, 1.0. Reported k, a, and Q/R values have a statistical fit greater than R^2 of 0.99.

For the three alloys without minor alloy addition, the oxidation rate of the base Fe-18Cr-18Mn alloy was not affected by the addition of interstitial nitrogen and/or nitrogen and carbon **(FIGURE 1)**. For the alloys with silicon, manganese, and nickel addition, there was almost an order of magnitude improvement in oxidation resistance. **(FIGURE 2)**. However, for alloys with minor alloy additions, the addition of carbon results in formation of chromium-carbide precipitates [8]. The precipitation of chromium carbides had a minor impact on oxidation resistance. The slightly lowering chromium solid solution concentration lowered the oxidation resistance. **(FIGURE 3)**.

X-ray diffraction analyses for oxide surfaces show the presence of both M_2O_3 sesquioxide and M_3O_4 spinel oxides for all samples **(TABLE III)**. There is little change in the peak position

(0.274 nm for the M_2O_3 and 0.296nm for M_3O_4) for any of the oxides regardless of alloy or test temperature suggesting the oxide compositions are essentially similar. The ratio of the maximum peak intensities for each oxide is used to provide a rough estimate of their relative concentrations of the different oxides. The dominant oxide is always M_2O_3.

X-ray diffraction beam energy was strong enough to penetrate through the oxides and into the metal substrate (**TABLE IV**). The metal phase at the metal-oxide interface was bcc. The presence of the bcc-phase was detected in all samples regardless of test temperature or alloy composition. The bcc phase lattice dimension was consistent, ≈0.203 nm, the same as the room temperature bcc lattice of the duplex phase base Fe-18Cr-18Mn alloy with no interstitial concentration. For the three alloys without minor alloy additions, the bcc phase was the only metallic phase observed. For the alloys with minor alloy additions, the oxide layer was thinner and the depth of X-ray diffraction into the metal was sufficient to penetrate through both the oxide and the surface bcc phases and into the bulk fcc phase. The fcc lattice dimension at room temperature was 0.209 nm.

Scanning electron micrographs of the oxide surface after 1244 hours at 525°C showed the development of the duplex oxide layer structure. The oxide structure for the alloys with minor alloy additions had the highest oxidation resistance and showed how the duplex oxide coatings start to grow and develop. The alloy with nitrogen only, alloy EA-1, had the lowest oxide weight gain. Its surface had three distinct regions: (1) a flat, smooth surface on the grain face, (2) rough surface profiling the outline of the grain boundaries, and (3) a few patches of accelerated oxidation with surface features similar to those of the oxide surface of the alloys with no minor alloying elements (**FIGURE 4A**). The two alloys with minor alloy components and with both nitrogen and carbon additions, alloys EA-2 and EA-3, had slightly higher oxidation rates. The oxide surface features that previously only outlined grain boundaries were greatly expanded and covered the majority of the grain surface (**FIGURE 4B**). The alloys with no minor additions, alloys A, B, and C, had significantly higher rates of oxidation and the outer surface oxide had formed a uniform coating (**FIGURE 4C**).

Scanning electron microscopic, selected-area, energy dispersive analysis of the outermost oxide surfaces measured an oxygen concentration of approximately 60 atomic percent, indicating the oxide to be a sesquioxide, M_2O_3, (**TABLE V**). The dominant metallic component of the surface oxide for all alloys at 525°C and 625°C and for alloys with minor alloy additions at 725°C was manganese with small contributions of iron and chromium. The outer oxide was characterized to be predominately Mn_2O_3. At 725°C, alloys with no minor alloy addition had a higher oxidation rate, sufficiently rapid to include a significant contribution of other base metal elements which formed a multi component sesquioxide, $(Mn,Fe,Cr)_2O_3$.

The depth of scanning electron microscopy penetration at 10kev acceleration potential was

approximately 0.4 to 0.5 microns, which limited characterization to the near-surface oxide layers. However, local spalling allowed selected-area scan examinations of subsurface oxide. **(TABLE VI, FIGURE 5)** SEM-EDX elemental analysis showed a manganese-dominated M_2O_3 sesquioxide surface oxide and a manganese-dominated M_3O_4 spinel inner oxide. The spinel layer was thick enough that it sometimes spalled or fractured in such manner as to characterize the chemical composition of the spinel as a function of thickness. The spinel chemical composition was not uniform but varied from a manganese-iron composition at the outer, spinel-sesquioxide interface to a manganese-iron-chromium composition at the metal-oxide interface.

DISCUSSION:

This study was designed to help define, characterize, and expand the environmental parameters in which interstitially-strengthened manganese stainless steels can operate. To date there have been a very limited number of studies of high-temperature applications of these alloys and their oxidation properties.

The oxide structure formed depends upon alloy composition. For chromium rich alloys (chromium concentration greater that n18 weight percent) that do not contain manganese, a single oxide, Cr_2O_3, forms [**9, 10, 11**]. For example, Fe-Cr-Ni stainless steels the dominant oxide formed is the highly oxidation protective sesquioxide, Cr_2O_3 [**12, 13**]. However, when the alloy contains manganese, even in concentrations as low as 1 weight percent, the manganese rapidly diffuses out and reacts with Cr_2O_3 and can form a thin outer spinel layer, $MnO{\bullet}Cr_2O_3$ or $MnCr_2O_4$ [**13, 14, 15**]. Development of a manganese-chromium spinel is desirable at moist elevated temperatures where Cr_2O_3 converts to gaseous $CrO_2(OH)_2$ [**16, 17**].

For Fe-Cr alloys that contain larger concentrations of manganese, a two layer sesquioxide - spinel forms. For bcc-Fe-Cr and Fe-Cr-Ni stainless steel alloys, the outer layer is the spinel, $MnCr_2O_4$, and the inner layer is the sesquioxide, Cr_2O_3 [**9, 12**]. For Fe-Cr-Mn alloys the outer oxide layer is Mn_2O_3 and the inner layer is $(Mn,Fe,Cr)_3O_4$ [**18, 19**]. This spinel layer is often chemically layered with the outer region manganese rich, the middle region iron rich, and the inner region chromium rich.

Several studies have explored diffusion and oxidation thermodynamics of iron-chromium-mananese alloys. The diffusion rate of manganese in spinel oxides and in fcc and bcc metal is greater than the diffusion rate of iron, chromium, or nickel [**18, 20**]. The rapid diffusion of manganese out of Fe-Cr-Mn stainless steels results in loss of the fcc phase and development of a bcc phase at the metal-oxide interface [**19, 21**]. The weight gain activation energy(Q/R) was for alloys in tis oxidation study were consistent with previous studies, suggesting the controlling mechanism was diffusion of oxygen in spinel oxides [**22, 23, 24,25**].

The three Fe-18Cr-18Mn alloys, one with no interstitials, one with nitrogen, and one with nitrogen and carbon, have nearly identical oxidation rates within experimental uncertainty **(FIGURE 1)**. Results suggest a slight increase in oxidation protection with the higher interstitial concentration (**TABLE II**). The oxides formed are stable and coherent after more than a thousand hours at 525°C and 625°C. However, at 725°C, spalling occurs. Minor alloy additions of silicon, molybdenum, and nickel significantly reduce the oxidation rate at all temperatures **(FIGURE 3)** and eliminate spalling at 725°C. The reduction of oxidation by minor alloy

addition of silicon and molybdenum has previously been studied **[14, 17, 26]**. However, minor alloy additions can have detrimental side effects. For example, alloying with silicon reduces carbon solubility, resulting in formation of $Cr_{23}C_6$ precipitates **[8]**. This loss of chromium from the solid solution reduces oxidation protection **(FIGURE 2)**.

The oxide structures developed in this study are consistent with those presented in previous iron-chromium-manganese alloy oxidation studies **[3, 4, 5, 18, 20, 27, 28, 29, 30, 31]**. X-ray diffraction showed the presence of spinel and sesquioxide phases. SEM-EDX chemical analyses showed a duplex oxide structure: the outer oxide to be manganese rich sesquioxide and the inner oxide to be manganese-iron-chromium spinel **(TABLE V and VI)**. The dominant oxide after an extended time was the outer sesquioxide phase.

Interstitial solubility of both nitrogen and carbon in bcc-Fe is significantly lower than in fcc-Fe. The lattice dimension for the interstitial free alloy at room temperature was 0.203 nm. This is essentially the same lattice dimension for the bcc-phase measured in the bulk metal at the metal-oxide interface after extended periods of oxidation, suggesting that the interstitials diffused out of the metal as the phase changed from bcc to fcc.

When the weight gain time and temperature data were combined and fitted to one equation (EQ.2), the oxidation rate constant '$\underline{a}$' varied between 0.001 and 0.52. The activation energy (Q/R) for oxidation for these alloys is within the range 12,000 to 20,000 . There are two sets of oxidation energies (Q/R) for these alloys: 14,000-15,000 for the base metal and base metal with only nitrogen and nitrogen carbon addition alloys, and 17,000-20,000 for the alloys with minor alloy additions. These values are consistent with parabolic energies determined in previous studies **[4, 5]**. Plotting ln($\underline{a}$) vs Q/R on a Compensation Effect relationship graph, also known as the Meyer-Neidel and Wert-Zener effect, **[32, 33, 34, 35]** there are two linear fits: one for the alloys with, and one for alloys without minor alloy additions **(FIGURE 6)**. The nearly identical slopes of the two lines indicate the same mechanism is controlling both sets of data. In other words, there is only one over-riding mechanism controlling the oxidation for all of the iron-chromium-manganese alloys in this study.

CONCLUSION

In this study, oxidation properties of Fe-18Cr-18Mn alloys were evaluatedat temperatures range 525 to 725°C. Fe-Cr-Mn alloys are of interest because they can accommodate large concentrations of interstitials and thereby, enhance many material properties such as strength, corrosion, and wear. This study showed that interstitial additions of nitrogen and of nitrogen and carbon do not affect the oxidation properties of Fe-18Cr-18Mn. Addition of minor solid-solution elements, silicon, molybdenum, and nickel, enhances the oxidation properties of Fe-18Cr-18Mn. However, the addition of these minor components reduces the solubility of carbon resulting in the formation of chromium carbides which slightly reduces oxidation protection.

The oxides formed in Fe-Cr-Mn are dominated by the presence of manganese and tend to form manganese based sesquioxide and spinel oxides which in certain environmental conditions provide more protection than Cr_2O_3 sesquioxide. The oxides formed in Fe-Cr-Mn have a duplex structure. The outer layer is a sesquioxide, M_2O_3 (M=Mn, Fe, Cr) with the dominate metallic component manganese. The inner layer is a spinel, M_3O_4 (M=Mn, Fe, Cr) with the chemical composition of the spinel varying from the metal-oxide interface outward. The outer most spinel is dominated by manganese, then inward the iron component increases, and at the metal interface, the chromium component increases. Development of these manganese-rich oxides results from the manganese diffusion out of the bulk metal and through the oxides. These manganese-rich spinel and sesquioxide oxides provide good oxidation protection. Loss of manganese from the metal matrix results in the transformation from fcc to bcc phase at the metal-oxide interface.

At 525°C and 625°C, Fe-18Cr-18Mn both with and without minor alloy additions maintain stable oxides. However at 725°C, alloys without minor alloy additions of silicon, molybdenum, and nickel spaulled, while those with minor alloy additions still maintained a stable oxide.

TABLES

Table I: Alloy Chemistry - phases - yield strength
Table II: Oxidation statistical Data - activation energy, k, a, etc.
Table III: XRD measurements of oxide lattice dimensions
Table IV: XRD measurements of bcc and fcc lattice dimensions
Table V: SEM-EDX surface oxide composition
Table VI: SEM-EDX oxide sub surface spalled oxide composition

FIGURES:

Figure 1: graph, $\delta[(wt/cm^2)]^2$ vs time, Fe-18Cr-18Mn with and without nitrogen and carbon interstitials: alloys A, B, and C at 525°C

Figure 2: graph $\delta[(wt/cm^2)]^2$ vs time, Fe-18Cr-18Mn with silicon, molybdenum, and nickel additions: alloys EA-1, -2, and -3 at 625°C

Figure 3: graph $\delta[(wt/cm^2)]^2$ vs time of alloys with and with out intersitials and with and without minor alloy additions A, C, EA-1, EA-3, at 525°C

Figure 4: SEM 3 micrographs: 525°C surface,
- 4A: EA1 - Lowest oxidation, surface had three distinct regions:
  - (1) a flat surface at the grain face,
  - (2) rough surface profile outlining the grain boundaries, and
  - (3) a few patches of accelerated oxidation with surface features similar to those of the oxide surface of the alloys with no minor alloying elements
- 4B: EA3 - Higher oxidation, surface features that previously only outlined grain boundaries were greatly expanded and covered the majority of the grain surface with but a few areas yet to be engulfed
- 4C: A - highest oxidation -oxide surfaces had formed a uniform coating.

Figure 5: Spaulled sub surface oxide structure

Figure 6: Meyer-Neidel or Wert-Zener, Compensation effect relationship Ln(A) vs Q/R graph

REFERENCES:

1 Oshima T., Habara Y., Kuroda K.
Materials Science Forum, vol. 539-43, pp.4897, 2007

2 Betencur-Rios J., Wang C., Nomura G., Perez-Alcazar G., Tabares J.
Hyperfine Interactions, vol.187, no.1-3, Nov. 2008

3 **F.Gesmundo, C. deAsmundia, G.Battilana, E.Ruedl**
Werkstoffe und Korrosion, vol.38, 1987, pp.367

4 **D.Doulass, F.Gesmundo, and C.deAsmundi**
Oxidation of Metals, vol. 25, no. 3-4, 1986, pp.235

5 **D.Douglass and F.Rizzo-Assuncao**
Oxidation of metals, vol.29, no.3-4, 1988, pp.271

6 **J.Rawers and N.Duttlinger**
Materials Science and Technology, vol.24, no.1, 2008, pp.97

7 **J.Rawers, J.Tylczak, D.Alman**
Tribology Transactions, vol.51, issue 4, pp.515, 2008

8 **J.Rawers**
Journal of Materials Science, vol.43, issue 10, pp.3618, 2008

9 **A.Sabioni, A.Huntz, E.daLuz, M.Mantel, C.Haut**
Materials Research, vol.6, no.2, 2003, pp.1352

10 **R.Wild**
Corrosion Science, vol.17, 1977, pp.87

11 **A.Paul, S.Elmrabet, J.Odriozoia**
Materials Science Forum, vol.383, 2002, pp.125

12 **H.Buscail, S.elMesski, F.Riffard, S.Perrier, R.Cueff, and C.Issartel**
Journal of Materials Science, vol. 43, no.21, 2008, pp.6960

13 **Z.Yang, J.Hardy, M.Walker, G.Xia, S.Simner, J.Stevenson**
Journal of Electrochemical society, vol.151, no.11, 2004, A1825

14 **J.Rawers and D.Larson**
Oxidation of Metals, vol.27, 1-2, 1987, pp.103

15 **P.Jian, H.Bing, G.Xie**
Journal of Power Sources, vol.158, Issue 1, 2006, pp.354

16 **G. R. Holcomb and D. E. Alman,**
Scripta Materialia, Vol. 54, Issue 10, May (2006) 1821-1825.

17 **A.Huntz, V.bague, G.Beauple, C.Haut.**
Applied Surface Science, vol. 207, Issue 1-4, 2003, pp.255

18 **J.Dudala, J.Gilewicz-Wolter, M.Wolter, M.Hetmanczyk,** "*The comparison of diffusion rates of chromium, manganese, and iron in Cr-Mn steels of austenitic, austenitic-ferritic, and ferritic structure*", conference. 1st international conf on diffusion in solids and liquids, 6-8 July 2005, Aveiro, Portugal

19 **J.Duh and J.Lee**

Journal of Electrochemistry Society, vol.136, no.3, 1989, pp.847
20 **J.Dudala, J.Gilewicz-Wolter, Z.Stegowski**
Diffusion and defect Forum, vol.237-240, part 2, 2005, pp.1199
21 **J.Kirkaldy, P.Smith. AndR.Sharma**
Metall. Trans., vol. 4, 1973, pp.624
22 **T.Horita, H.Kishhinoto,**
Solid State Ionics, vol. 179, issue 38, 2008, pp.2216
23 **J.Castle and P.Surman**
Journal of Physical Chemistry, vol.71, no.13, 1967, pp.4255
24 **K.Reedy and A.Cooper**
Journal of the American Ceramic Society, vol.66, issue 9, 1983, pp.664
25 **T.Horita, K.Yamaji, Y.Xiong, H.Kishimoto, N.Sakai, H.Yokokawa**
Solid State Ionics, vol.175, issue 1-4, 2004, pp.157
26 **D.Caplan, P.Beaubien, and M.Cohen**
Trans. Metall. Society AIME, vol.233, 1965, pp.766
27 **R.Matera and E.Ruedl,**
Werstoffe und Korrosion vol. 40, 1989, pp 206
28 **A.Marasco and D. Young**
Oxidation of Metals, vol.36, nos. 1-2, 1991 p. 157
29 **Z.Zurek, J.Gilewicz-Wolter, M.Hetmanczyk, J.Dudala, A.Stawiarski**
Oxidation of Metals, vol.64, no.5-6, 2005, pp.379
30 **J.Gilewicz-Wolter, Z.Zurek, J. Dudala, J.Lis, M.Homa, and M.Wolter**
Advances in Science and Technology, vol.46, 2006, pp.27
31 **J.Gilewicz-Wolter, Z. Zurek, J.Dudala, J.Lis, M.Homa, M.Wolter**
Journal of Phase Equilibrium and Diffusion, vol.26, no.5, 2005, pp.561
32 **J.Philibert**
Defect and diffusion forum, vol. 249, 2006, pp.61
33 **T.Dosdale and R.Brook**
Journal of American Ceramic Society, vol. 66, issue 6, 1983, pp.392
34 **W.Meyer & H.Neidel**
Z.Tech.Phys, vol.18, 1937, p.588
35 **C.Wert & C.Zener**
Phys. Rev., vol.76, 1949, p.1149

TABLE I: Ingot Chemistry

Sample	Fe	Cr wt%	Mn wt%	Ni wt%	Si wt%	Mo wt%	N wt%	C wt%	Matrix	fcc-lattice nm	σ_{YIELD}, MPa
A	bal.	17.9	17.7	0.0	0.0	0.00	0.0	0.01	fcc - bcc	0.3594	339
B	bal.	17.9	17.1	0.0	0.0	0.0	0.56	0.03	fcc	0.3618	598
C	bal.	17.5	18.2	0.0	0.0	0.0	0.43	0.46	fcc	0.3622	679
EA-1	bal.	16.1	17.8	1.9	0.3	0.9	0.58	0.04	fcc	0.3621	624
EA-2	bal.	17.4	17.6	1.8	0.3	0.9	0.52	0.44	fcc -$M_{23}C_6$	0.3622	668
EA-3	bal.	16.2	17.6	1.8	0.4	0.8	0.63	0.64	fcc -$M_{23}C_6$	0.3622	680

TABLE II: $\delta[(g/cm^2)]^2 = k(x10^{-12})\bullet t(hours) = a\bullet exp^{(-Q/RT)}\bullet t$

	total weight gained/area			oxidation constant, k			parabolic oxidation	
	525°C	625°C	725°C	525°C	625°C	725°C	a	Q/R
A	0.29	1.71	0.24	100.0	2760	15400*	0.029 ±0.04	14625 ±650
B	0.32	1.59	0.18	128	2390	11400*	0.014 ±0.03	14074 ±606
C	0.27	1.35	0.10	172	2350	11000*	0.063 ±0.23	15430 ±1542
EA-1	0.04	0.29	0.37	3.3	81	202	0.0001 ±0.00	11756 ±680
EA-2	0.12	0.39	0.72	16	156	1190	0.025 ±0.06	17068 ±468
EA-3	0.15	0.39	0.77	29	161	1280	0.520 ±0.02	19836 ±394
test, hrs	1244		1244		670			

* spalled before end of tests

TABLE III: Oxide lattice dimensions, nm

	M_2O_3			M_3O_4		
	525°C	625°C	725°C	525°C	625°C	725°C
A	0.274	0.272 0.274	0.272	0.250	0.256	0.254
B	0.274	0.273 0.274	0.272	0.250	0.256	0.254
C	0.274	0.273	0.272	0.249	0.256	0.252
EA-1	0.273	0.273	0.273		0.257	0.258
EA-2	0.274	0.273	0.273		0.257	0.257
EA-3	0.273	0.273	0.273		0.257	0.257

(Mn_2O_3 = 0.272, Mn_2FeO_4 = 0.249, Fe_2MnO_4 = 0.256/7, Cr_3O_4 = 0.258)

TABLE IV: Surface metal lattice: X-Ray Diffraction

	R.T.	**525°C**	**626°C**	**725°C**	
A	0.203 0.208	0.203	0.203	0.203	bcc fcc
B	0.209	0.203	0.203	0.203	bcc fcc
C	0.209	0.203	0.203 0.208	0.203	bcc fcc
EA-1	0.209	0.204 0.209	0.203 0.209	0.203 0.208	bcc fcc
EA-2	0.209	0.204 0.208	0.203 0.208	0.203 0.207	bcc fcc
EA-3	0.209	0.203 0.209	0.203 0.208	0.203	bcc fcc

TABLE V: SEM-EDX Overall oxide surface chemistry

	525°C				625°C				725°C			
	Fe	Cr	Mn	O	Fe	Cr	Mn	O	Fe	Cr	Mn	O
A	4.1	9.7	26.3	59.9	2.0	4.4	32.5	61.0	10.5	11.3	18.4	59.8
B	5.0	7.3	27.8	60.0	1.9	2.3	35.4	60.4	10.7	3.5	24.3	59.1
C	4.7	5.1	29.6	60.6	1.8	1.5	36.1	58.4	22.7	2.7	13.7	59.2
EA-1	10.3	12.0	22.3	55.0	1.1	4.2	33.3	61.4	0.9	5.7	28.9	60.3
EA-2	3.4	6.4	28.4	61.3	1.4	3.0	32.0	61.2	7.2	4.6	26.7	58.9
EA-3	4.7	7.4	27.4	60.3	1.3	3.4	32.2	61.4	12.0	2.1	23.7	59.6

TABLE VI: SEM - EDX Chemistry of Spalled oxide layers from 725°C test

	Outer - Sesquioxide			Middle - Spinel			Deepest - Spinel		
	F	Cr	Mn	Fe	Cr	Mn	Fe	Cr	Mn
A	3	4	35	25	4	14	17	21	5
B	4	7	28						
C	5	4	30				18	20	2
EA-1	1	7	31	10	8	23	10	23	12
EA-2	4	7	28	13	5	24	12	25	10
EA-3	5	7	27				12	24	3

Figure 1: Effect of interstitial nitrogen and carbon addition on oxidation properties of Fe-18Cr-18Mo temperature 625°C. Weight gained $\delta[(wt/cm^2)]^2$ vs time (hours)

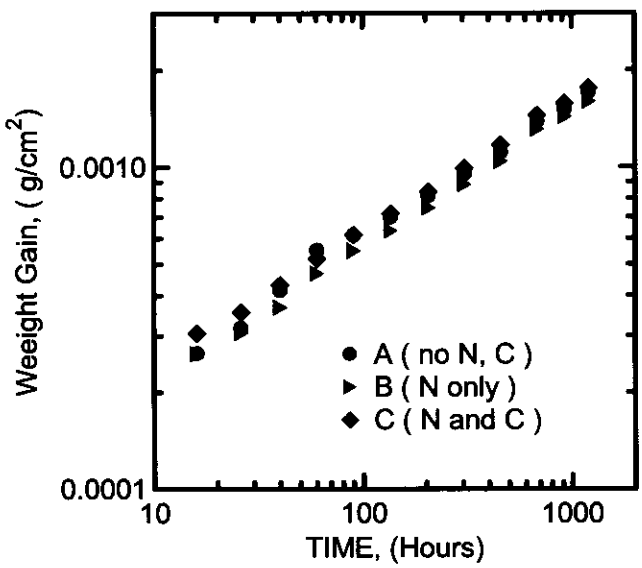

FIGURE 2: Effect of nitrogen and carbon addition on oxidation properties of Fe-18Cr-18Mo with minor additions of 0.3 wt% silicon, 0.9 wt% molybdenum, and 0.6 wt% nickel at a temperature of 625°C. Weight gained $\delta[(wt/cm^2)]^2$ vs time (hours)

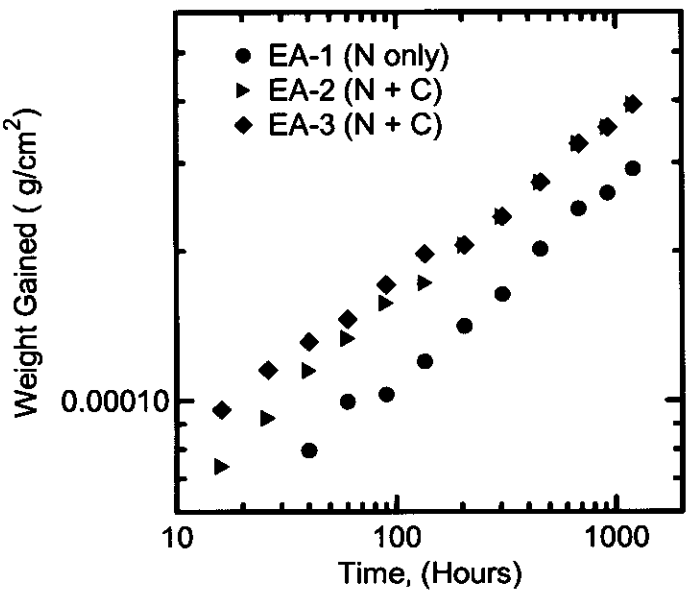

Figure 3: Effect of nitrogen and nitrogen plus carbon addition on oxidation properties of Fe-18Cr-18Mo with and without minor additions of 0.3 wt% silicon, 0.9 wt% molybdenum, and 0.6 wt% nickel at a temperature of 525°C. Alloy EA-2 formed Cr23C6 precipitates and thus reduced the chromium solute concentration. Weight gained $\delta[(wt/cm^2)]^2$ vs time (hours)

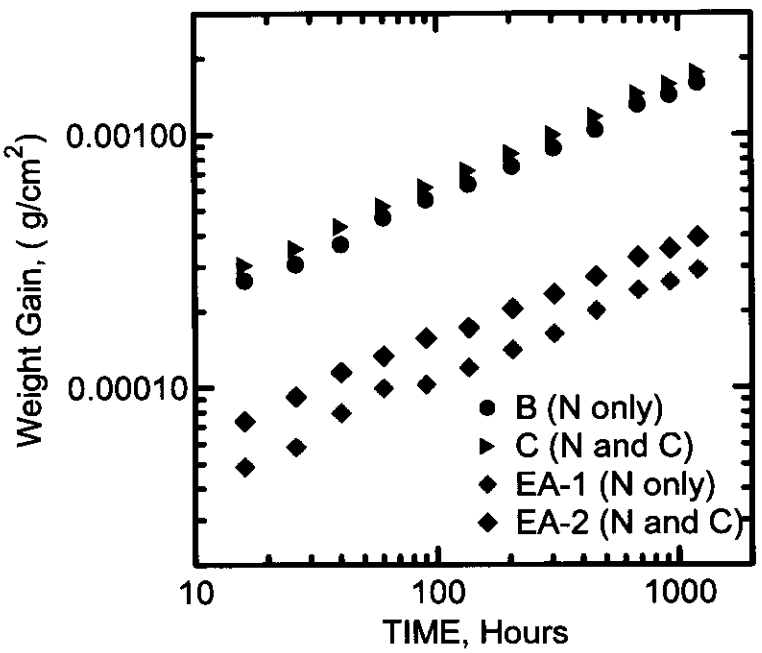

Figure 4C

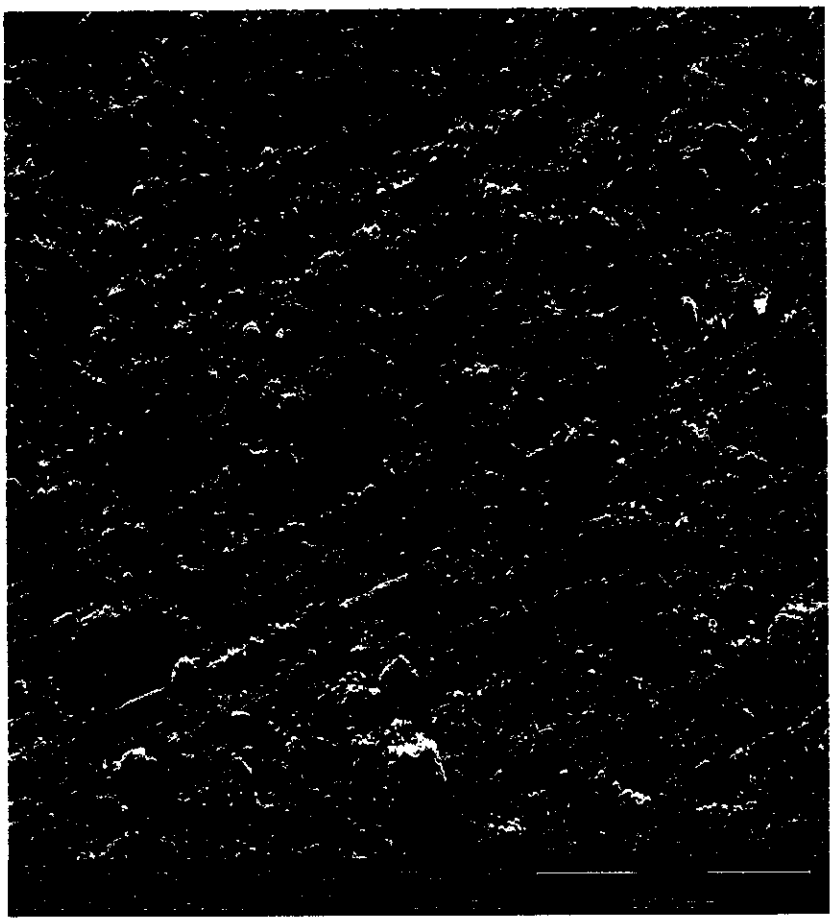

Figure 4B

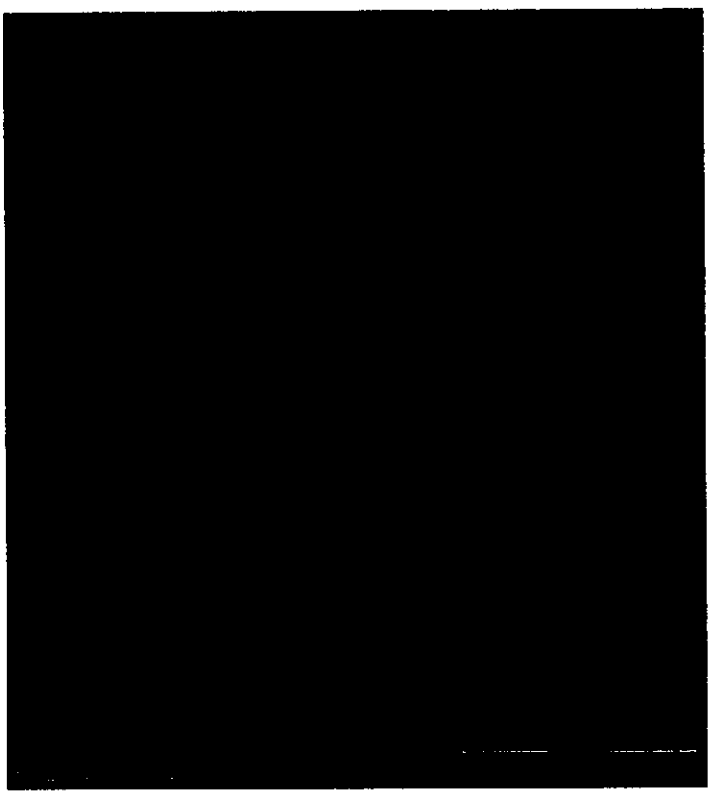

FIGURE 4A

Figure 5

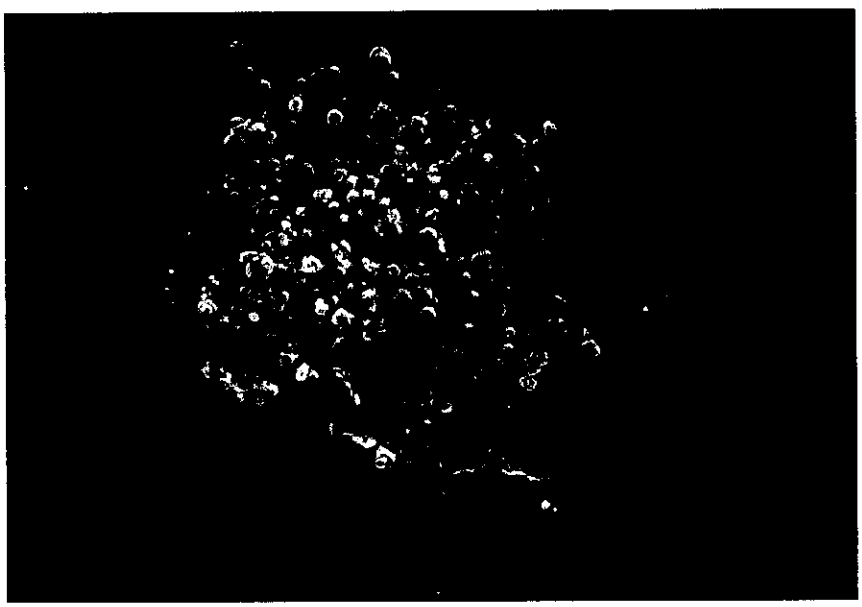

FIGURE 6 Meyer-Neidel or Wert-Zener Compensation effect relationship Ln(A) vs Q/R graph

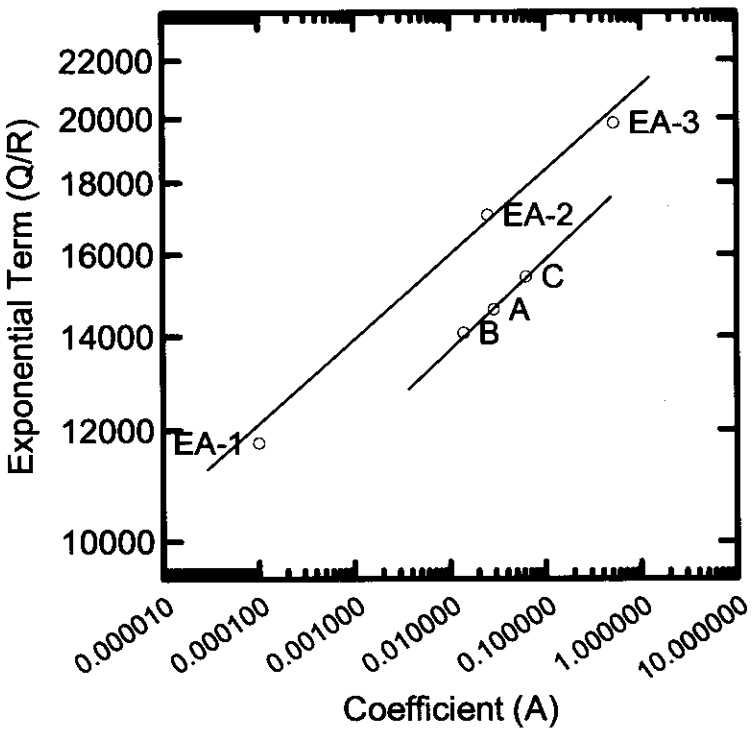

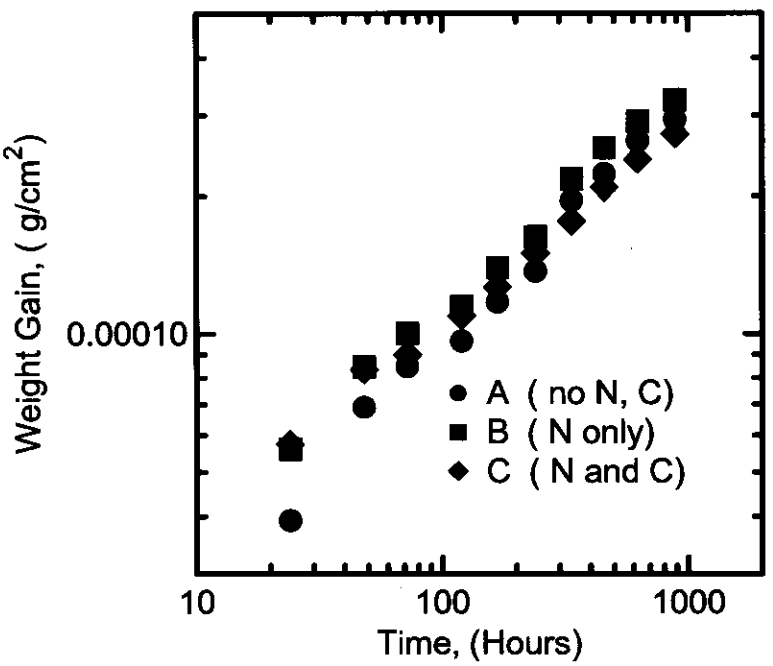
Weight Gain, (g/cm^2)
0.00010
10
100
1000
Time, (Hours)
A (no N, C)
B (N only)
C (N and C)